





Atomic dynamics of metallic glass melts $\text{La}_{50}\text{Ni}_{15}\text{Al}_{35}$ and $\text{Ce}_{70}\text{Cu}_{19}\text{Al}_{11}$ studied by quasielastic neutron scattering

Peng Luo ¹, Abhishek Jaiswal,^{1,2} Yanqin Zhai,^{1,2} Zhikun Cai,^{1,2} Nathan P. Walter ^{1,2}, Long Zhou,^{1,2} Dawei Ding,^{3,7} Ming Liu,³ Rebecca Mills,⁴ Andrey Podlesynak ⁴, Georg Ehlers,⁵ Antonio Faraone,⁶ Haiyang Bai,^{3,7} Weihua Wang,^{3,7} and Y Z ^{1,2,8,*}

¹Beckman Institute for Advanced Science and Technology, University of Illinois at Urbana-Champaign, Urbana, Illinois 61801, USA

²Department of Nuclear, Plasma, and Radiological Engineering, University of Illinois at Urbana-Champaign, Urbana, Illinois 61801, USA

³Institute of Physics, Chinese Academy of Sciences, 100190 Beijing, China

⁴Neutron Scattering Division, Oak Ridge National Laboratory, Oak Ridge, Tennessee 37831, USA

⁵Neutron Technologies Division, Oak Ridge National Laboratory, Oak Ridge, Tennessee 37831, USA

⁶NIST Center for Neutron Research, National Institute for Standards and Technology, Gaithersburg, Maryland 20899, USA

⁷Songshan Lake Materials Laboratory, Dongguan, Guangdong 523808, China

⁸Department of Electrical and Computer Engineering, University of Illinois at Urbana-Champaign, Urbana, Illinois 61801, USA



(Received 26 January 2021; revised 2 May 2021; accepted 14 June 2021; published 23 June 2021)

By employing quasielastic neutron scattering, we studied the atomic-scale relaxation dynamics and transport mechanism of $\text{La}_{50}\text{Ni}_{15}\text{Al}_{35}$ and $\text{Ce}_{70}\text{Cu}_{19}\text{Al}_{11}$ metallic glass melts in the temperature range of >200 K above their liquidus temperatures. The results show that both liquids exhibit stretched exponential relaxation and Arrhenius-type temperature dependence of the effective diffusion coefficient. The $\text{La}_{50}\text{Ni}_{15}\text{Al}_{35}$ melt exhibits an activation energy of 0.545 ± 0.008 eV and a stretching exponent ~ 0.77 to 0.86 in the studied temperature range; no change of activation energy, as suggested in previous reports, associated with liquid-liquid phase transition was observed. In contrast, the $\text{Ce}_{70}\text{Cu}_{19}\text{Al}_{11}$ melt exhibits larger diffusivity with a much smaller activation energy of 0.201 ± 0.003 eV and a smaller stretching exponent ~ 0.51 to 0.60 , suggestive of more heterogeneous dynamics.

DOI: [10.1103/PhysRevB.103.224104](https://doi.org/10.1103/PhysRevB.103.224104)

I. INTRODUCTION

Metallic glasses (MGs) represent unique and fascinating materials that possess superior mechanical and functional performances [1–3]. Since the fabrication of AuSi MG by Klement *et al.* [4], a large variety of multicomponent MGs have been developed, such as Pd-, Pt-, Zr-, Mg-, Au-, and Fe-based and various rare-earth-based MG systems [1]. MGs are often produced by rapid quenching of liquid alloy that avoids the occurrence of crystallization and retains the amorphous liquid structure into a nonequilibrium rigid state. Therefore, the understanding of the atomic relaxation processes and transport mechanism in the equilibrium liquid state is important to elucidate the nucleation and crystal growth [5,6], the glass formation [7,8], as well as the physical properties of the glassy state [9–11].

The characteristic timescale of atomic motions in liquid alloys is on the order of picoseconds, which can be well covered by quasielastic neutron scattering (QENS) [12]. Therefore, QENS has been extensively used to study the relaxation dynamics and transport properties of liquid alloys, revealing that the relaxation dynamics of multicomponent glass-forming metallic liquids exhibits a stretched exponential behavior even in the equilibrium state [13–23], in contrast to the case of

some other liquids such as water and aqueous solutions [24]. This is a manifestation of the heterogeneous dynamics associated with the intrinsic chemical disorder and inhomogeneous local environment of the glass-forming metallic liquids composed of multiple elements with distinct atomic sizes [25].

Rare-earth-based MGs provide model systems for the study of the mechanical deformation [26–29], the slow structural relaxation [30–33], and the fast dynamic processes of MGs [34–43]. The LaNiAl system shows pronounced Johari-Goldstein β relaxation well separated from the primary α process [37,44,45] and has been extensively used to study the correlation between β relaxation and other important properties of MGs [26,32,33,37,46–48]. In a recent nuclear magnetic resonance study of glass-forming $\text{La}_{50}\text{Ni}_{15}\text{Al}_{35}$ melt, Xu *et al.* [49] suggested the occurrence of a change of the activation energy of diffusivity accompanying a liquid-liquid phase transition in the equilibrium liquid state. Another interesting and extensively studied CeCuAl system, called amorphous metallic plastic [50], exhibits exceptionally low glass transition temperature and polymerlike thermoplastic deformability in near-boiling water. Fundamental understanding of these important properties of rare-earth-based MGs and melts requires knowledge of atomic dynamics in the liquid state; however, direct experimental measurements are rare.

In this paper, we employed QENS to study the microscopic liquid dynamics of two prototypical rare-earth-based MG-forming melts $\text{La}_{50}\text{Ni}_{15}\text{Al}_{35}$ and $\text{Ce}_{70}\text{Cu}_{19}\text{Al}_{11}$. While

*Corresponding author: zhyang@illinois.edu

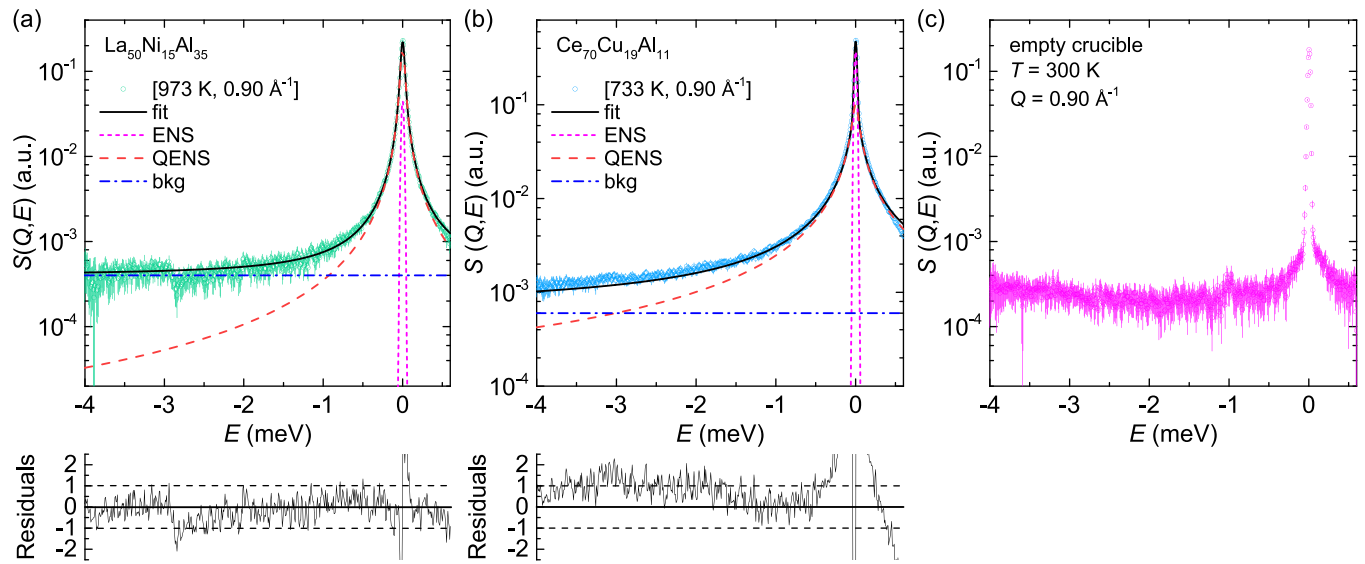


FIG. 1. Dynamic structure factor $S(Q = 0.90 \text{ \AA}^{-1}, E)$ of (a) $\text{La}_{50}\text{Ni}_{15}\text{Al}_{35}$ melt at 973 K, (b) $\text{Ce}_{70}\text{Cu}_{19}\text{Al}_{11}$ melt at 733 K, and (c) empty crucible at 300 K. Solid lines are fits with the Kohlrausch-Williams-Watts (KWW) model described in Eqs. (1) and (2). The room temperature measurement of the empty crucible is taken as the instrumental resolution and the elastic component [elastic neutron scattering (ENS), dotted line]. Dashed line denotes the Fourier transform of the KWW component [quasielastic neutron scattering (QENS)], and dash-dotted line represents the constant background (bkg). The lower panels in (a) and (b) show the normalized residuals defined as $(\text{data} - \text{fit})/\text{error}$.

the former has an intermediate fragility, the latter is a stronger glass-forming system [51–53]. The results show that both liquids exhibit stretched exponential relaxation, and the diffusion coefficients follow Arrhenius temperature dependence in the temperature range probed. However, the change of activation energy, as suggested in Ref. [49], associated with liquid-liquid phase transition was not observed for $\text{La}_{50}\text{Ni}_{15}\text{Al}_{35}$. Compared with the $\text{La}_{50}\text{Ni}_{15}\text{Al}_{35}$ liquid, the $\text{Ce}_{70}\text{Cu}_{19}\text{Al}_{11}$ liquid shows much smaller activation energy and more stretched shape of the scattering law, suggestive of more complex relaxation dynamics.

II. EXPERIMENTAL METHODS

A. Materials

Alloys with atomic compositions $\text{La}_{50}\text{Ni}_{15}\text{Al}_{35}$ (glass transition temperature $T_g = 528 \text{ K}$, liquidus temperature $T_L = 970 \text{ K}$ [49]) and $\text{Ce}_{70}\text{Cu}_{19}\text{Al}_{11}$ ($T_g = 341 \text{ K}$, $T_L = 722 \text{ K}$ [54]) were firstly prepared by arc melting of raw materials and subsequently cast in a water-cooled copper mold in a Ti-getter high-purity ($\geq 99.999\%$) argon atmosphere, forming a glassy rod 30 mm long and 2 mm in diameter. The purity of the raw materials in weight percent is listed as follows: La (99.9%), Ce (99.5%), Al (99.999%), Ni (99.995%), Cu (99.9999%), and Nb (99.95%).

B. QENS

QENS measurements were carried out at the Cold Neutron Chopper Spectrometer [55] at the Spallation Neutron Source at Oak Ridge National Laboratory. We used a MgO crucible as a sample container because it shows no significant reactions with the studied materials in liquid state. The samples were stacked in a cylindrical MgO container (2.4 mm wall thickness and 12.7 mm inner diameter) with an MgO rod insert (7 mm

diameter), which creates an annular sample geometry with a thickness of 2.85 mm. At this sample geometry, multiple scattering can be highly reduced. The crucible was suspended to the thermocouples using thin niobium wires inside a high-temperature furnace. A high-purity inert helium gas in a high vacuum ($\sim 10^{-3} \text{ Pa}$) was maintained during the measurements. Two thermocouples were used at various locations to verify the uniformity of temperature inside the furnace. The measurements were carried out in the temperature range of 973–1183 K in steps of 30 K for $\text{La}_{50}\text{Ni}_{15}\text{Al}_{35}$ and 733–983 K in steps of 25 K for $\text{Ce}_{70}\text{Cu}_{19}\text{Al}_{11}$. A low-energy incident neutron beam of 1.55 meV was used in the “High Flux” operational mode of the choppers. A measurement of the empty MgO crucible at room temperature yields the instrumental energy resolution function that is described well by a Gaussian function with an energy resolution of $\sim 25 \mu\text{eV}$ full width at half maximum. The studied wave vector transfer Q range was $0.19\text{--}1.35 \text{ \AA}^{-1}$. This is well below the structure factor maximum Q_0 at $\sim 2.4 \text{ \AA}^{-1}$ for both $\text{La}_{50}\text{Ni}_{15}\text{Al}_{35}$ and $\text{Ce}_{70}\text{Cu}_{19}\text{Al}_{11}$ [15,49]; hence, the scattering is a combination of spin, isotopic, and elemental incoherence [17]. At a specific temperature, data were collected for $\sim 4 \text{ h}$ to obtain good counting statistics. The total scattered neutron intensity spectrum was corrected for the time-independent background and normalized by the white-beam vanadium run, resulting in the dynamic structure factor $S(Q, E)$.

III. RESULTS AND DISCUSSION

Figure 1 displays the typical quasielastic signal of $S(Q = 0.9 \text{ \AA}^{-1}, E)$ for $\text{La}_{50}\text{Ni}_{15}\text{Al}_{35}$ at 973 K [Fig. 1(a)] and $\text{Ce}_{70}\text{Cu}_{19}\text{Al}_{11}$ at 733 K [Fig. 1(b)], as well as the empty can [Fig. 1(c)], in a semilogarithmic representation. The broadening of the spectrum with respect to the elastic scattering peak reflects the energy transfers between the scattered

neutrons and the moving atoms at specific wave vector transfer, thus providing information on the microscopic liquid dynamics. The measured $S(Q, E)$ spectra were analyzed in terms of the sum of an elastic component and Fourier transform of the Kohlrausch-Williams-Watts (KWW) stretched exponential function, convoluted with the instrumental resolution $R(Q, E)$, plus a constant background (bkg):

$$S(Q, E) = A[f\delta(E) + (1 - f)\mathcal{F}\{F(Q, t)\}] \otimes R(Q, E) + \text{bkg}, \quad (1)$$

where A represents the area of the spectrum, f is the fraction of the elastic scattering component arising from the sample container and/or the dynamics of the sample slower than the instrument resolution; $F(Q, t)$ is the intermediate scattering function, modeled as

$$F(Q, t) = \exp\left[-\left(\frac{t}{\tau}\right)^\beta\right], \quad (2)$$

where τ is the Q -dependent relaxation time, and β the stretching exponent. The various components of the fitted curve are also presented in Fig. 1. At the studied temperatures, the detailed balance factor is negligible in the measured dynamic range. The data were initially fitted using an arbitrary value of f , τ , β , and bkg. At each temperature, β was found to show only a small variation with a standard error of ≤ 0.05 without any systematic trend with Q [56]. The fitted f also shows no obvious Q dependence, and bkg is almost constant independent of both Q and temperature. Therefore, subsequent analysis was carried out by fixing the values of f and β to the average values at each temperature, and bkg was fixed at the average values 4×10^{-4} for $\text{La}_{50}\text{Ni}_{15}\text{Al}_{35}$ and 6×10^{-4} for $\text{Ce}_{70}\text{Cu}_{19}\text{Al}_{11}$ at the studied Q and temperature ranges. This fitting procedure yields a more reasonable value of τ at the low Q values ($< 0.5 \text{ \AA}^{-1}$), where the dynamic range is rather limited compared with that at higher Q ; otherwise, the fitted τ at $Q < 0.5 \text{ \AA}^{-1}$ falls outside the trend. We emphasize that the same results will be obtained if we ignore the data at $Q < 0.5 \text{ \AA}^{-1}$ and perform the fitting without any constraints on the parameters (Fig. S1 in the Supplemental Material [57]).

Figure 2 displays representatively the measured dynamic structure factor for the studied materials at different temperatures and at different wave vector transfers, being normalized by the peak height $S(Q, 0)$ for better comparison. Linear representation of $S(Q, E)$ without normalization was shown in Figs. S2–S5 of the Supplemental Material [57]. As temperature increases, the $S(Q, E)$ spectra show increasingly enhanced broadening due to the escalating atomic mobility in the liquids [Figs. 2(a) and 2(b)]. As the incident neutron energy is comparable with the energy transfers for atomic motions, the accessible kinematic region varies at each Q value [58], as seen in Figs. 2(c) and 2(d). In the studied Q range from 0.19 – 1.35 \AA^{-1} , an increasing broadening of the $S(Q, E)$ spectrum is observed [Figs. 2(c) and 2(d)], indicating wave vector transfer dependence of the relaxation time. Note that there exists a small glitch on $S(Q, E)$ around $E = -3 \text{ meV}$ independent of both temperature and Q (see Figs. 1 and 2). To verify that this small glitch does not affect the data analysis, we fitted only the $S(Q, E)$ spectra at $E > -2 \text{ meV}$, leaving all the parameters free. Consistent results were obtained with and

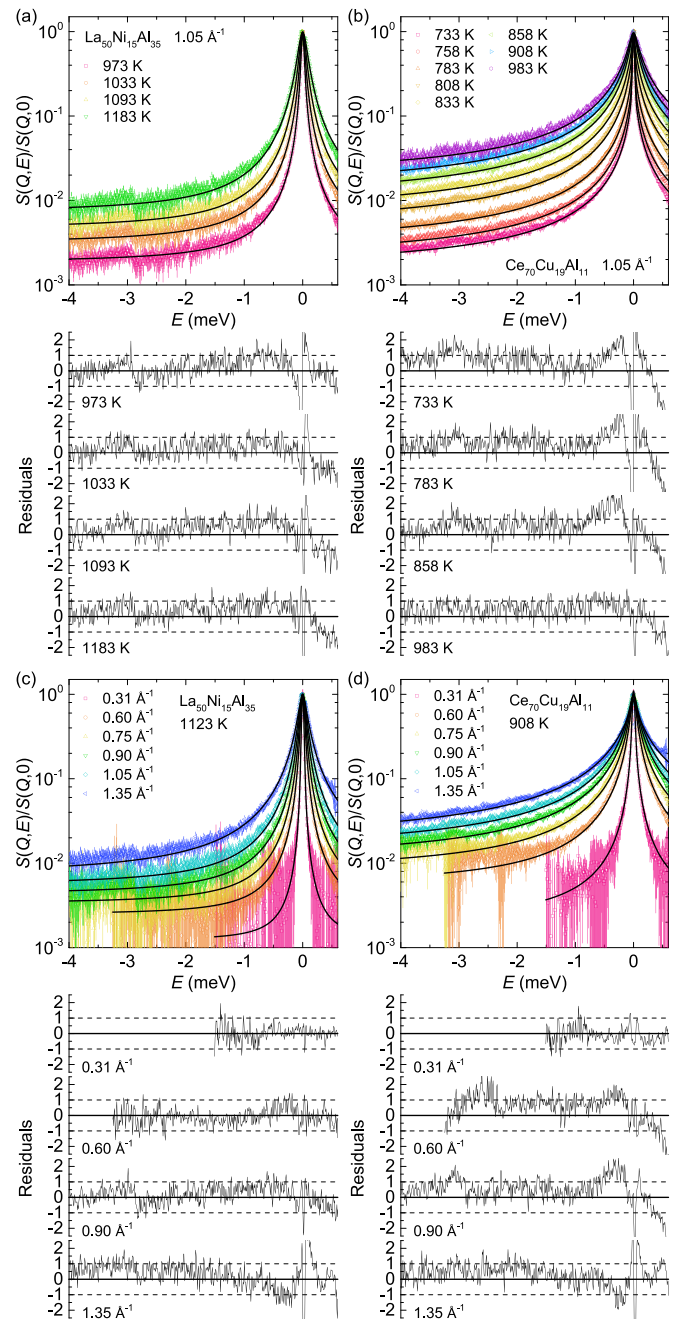


FIG. 2. Representative $S(Q, E)/S(Q, 0)$ of (a) and (c) $\text{La}_{50}\text{Ni}_{15}\text{Al}_{35}$ and (b) and (d) $\text{Ce}_{70}\text{Cu}_{19}\text{Al}_{11}$ melts at different Q and temperatures as denoted. Solid lines are fits with the Kohlrausch-Williams-Watts (KWW) model. The lower panel in each figure shows the representative normalized residuals defined as (data – fit)/error.

without considering this glitch (Fig. S1 in the Supplemental Material [57]).

The Q -dependent relaxation times obtained from the KWW fittings are in the range of 3 – 300 ps for $\text{La}_{50}\text{Ni}_{15}\text{Al}_{35}$ [Fig. 3(a)] and 0.8 – 100 ps for $\text{Ce}_{70}\text{Cu}_{19}\text{Al}_{11}$ [Fig. 3(b)] across the various Q and temperature values, corresponding to the slow α relaxation in the system [17,59,60]. The stretching exponent β of $\text{La}_{50}\text{Ni}_{15}\text{Al}_{35}$ liquid is larger than that of

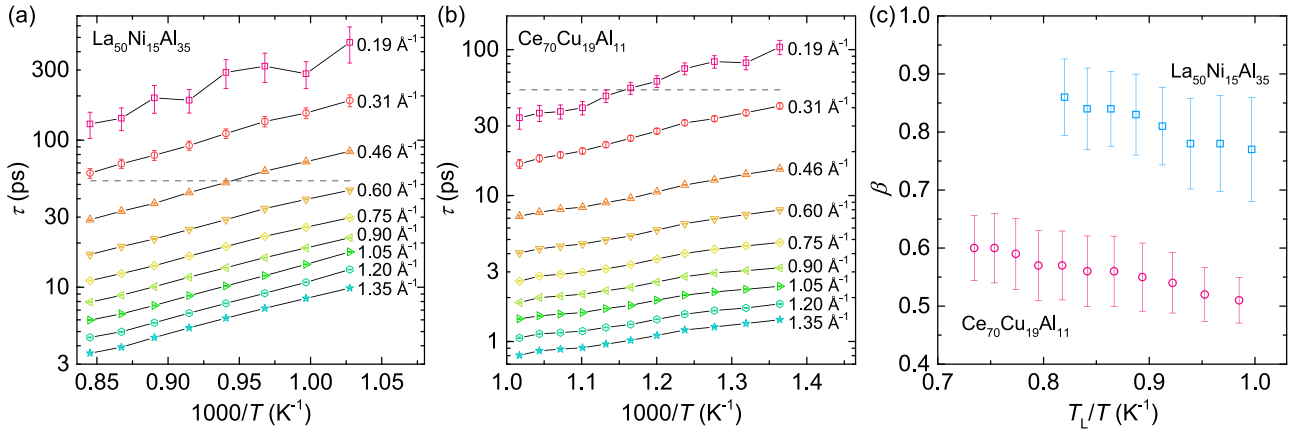


FIG. 3. (a) and (b) Relaxation time τ as a function of the inversed temperature $1000/T$ at different Q for (a) $\text{La}_{50}\text{Ni}_{15}\text{Al}_{35}$ and (b) $\text{Ce}_{70}\text{Cu}_{19}\text{Al}_{11}$ melts. The dashed lines in (a) and (b) indicate the resolution of the measuring configuration. (c) Stretching exponent β as a function of T_L/T for both melts.

$\text{Ce}_{70}\text{Cu}_{19}\text{Al}_{11}$, and it shows a gradual change with temperature [Fig. 3(c)]: for $\text{La}_{50}\text{Ni}_{15}\text{Al}_{35}$, β decreases from 0.86 to 0.77 as temperature decreases from 1183 to 973 K; for $\text{Ce}_{70}\text{Cu}_{19}\text{Al}_{11}$, it decreases from 0.60 to 0.51 as temperature decreases from 983 to 733 K. The relaxation behavior of liquids above T_L is usually characterized by simple exponential relaxation, such as in water and aqueous solutions [24], and in some monatomic [61–66] and binary metallic liquids [67–73]. In most cases of multicomponent metallic liquids, the relaxation process exhibits a stretched exponential behavior [13–15, 17–23].

Stretched exponential relaxation is usually explained by two limiting scenarios [74]: the “homogeneous” one considering that all of the particles in the system relax identically but by an intrinsically nonexponential process, and the “heterogeneous” one related to the superposition of different simple exponential relaxations weighted by a broad distribution of relaxation times. In the case of homogeneous dynamics, $\tau^\beta \propto Q^{-2}$ is expected, and in the heterogeneous scenario, the dynamics follows $\tau \propto Q^{-2}$ [74]. As will be seen in Fig. 4, the mean relaxation times agree with Q^{-2} dependence. Since β is independent of Q , $\tau \propto Q^{-2}$ is expected for both materials in the studied temperature and Q ranges, hence agreeing with the heterogeneous scenario. Therefore, the presence of

stretched exponential relaxation even in the equilibrium liquid state could be related to the increased number of constituents leading to enhanced local chemical variation and thus heterogeneous dynamics with individual relaxing units in the system having site-specific relaxation times. In that regard, the smaller value of β in $\text{Ce}_{70}\text{Cu}_{19}\text{Al}_{11}$ than in $\text{La}_{50}\text{Ni}_{15}\text{Al}_{35}$ implies stronger local chemical bias and more heterogeneous dynamics. The decrease of β with decreasing temperature suggests increased dynamic heterogeneity at slower atomic motions, which is supposed to result in an increasing number of slow contributions to the dynamics that are slower than the instrument resolution, in accord with the observed increase of f as the temperature is lowered (Fig. S6 in the Supplemental Material [57]).

The mean relaxation times were calculated using the following equation:

$$\langle \tau \rangle = \int_0^\infty dt F(Q, t) = \tau \beta^{-1} \Gamma(\beta^{-1}), \quad (3)$$

where $\Gamma(x)$ is the Γ function. In Fig. 4, $1/\langle \tau \rangle$ is plotted against Q^2 for the $\text{La}_{50}\text{Ni}_{15}\text{Al}_{35}$ liquid [Fig. 4(a)] and for the $\text{Ce}_{70}\text{Cu}_{19}\text{Al}_{11}$ liquid [Fig. 4(b)] at different temperatures. We can see $1/\langle \tau \rangle \propto Q^2$ in the studied Q range up to 1.35 \AA^{-1} , as one would expect in the hydrodynamic limit for $Q \ll Q_0$ [58]. This allows us to evaluate an effective diffusion coefficient $D = 1/\langle \tau \rangle Q^2$.

In Fig. 5, we present the effective diffusion coefficient D as a function of T_L/T for better comparison of the systems with different T_L . In the studied temperature ranges for both alloy liquids, the diffusion coefficients follow an Arrhenius temperature dependence:

$$D = D_0 \exp\left(-\frac{\Delta E}{k_B T}\right), \quad (4)$$

where ΔE marks the activation energy, k_B is the Boltzmann constant, and D_0 is the exponential prefactor. The corresponding Arrhenius fits to the measured data presented by solid lines in Fig. 5 give an activation energy $\Delta E = 0.545 \pm 0.008 \text{ eV}$ and a prefactor $D_0 = 30.5 \pm 2.6 \text{ \AA}^2 \text{ ps}^{-1}$ for $\text{La}_{50}\text{Ni}_{15}\text{Al}_{35}$, while $\text{Ce}_{70}\text{Cu}_{19}\text{Al}_{11}$ exhibits much weaker temperature dependence with $\Delta E = 0.201 \pm 0.003 \text{ eV}$ and $D_0 = 4.8 \pm 0.2 \text{ \AA}^2 \text{ ps}^{-1}$.

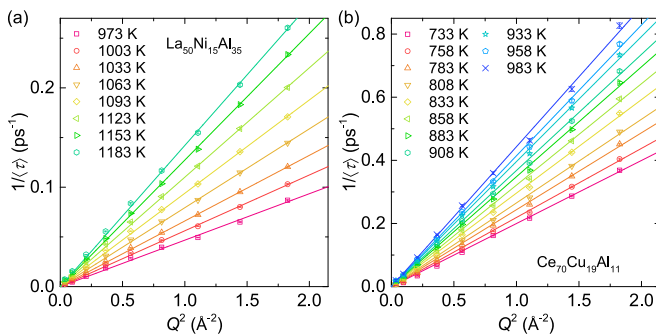


FIG. 4. Q^2 dependence of the inversed average relaxation time $\langle \tau \rangle$ for (a) $\text{La}_{50}\text{Ni}_{15}\text{Al}_{35}$ and (b) $\text{Ce}_{70}\text{Cu}_{19}\text{Al}_{11}$ at different temperatures. The straight lines are linear fits, and the slope gives the effective diffusion coefficient.

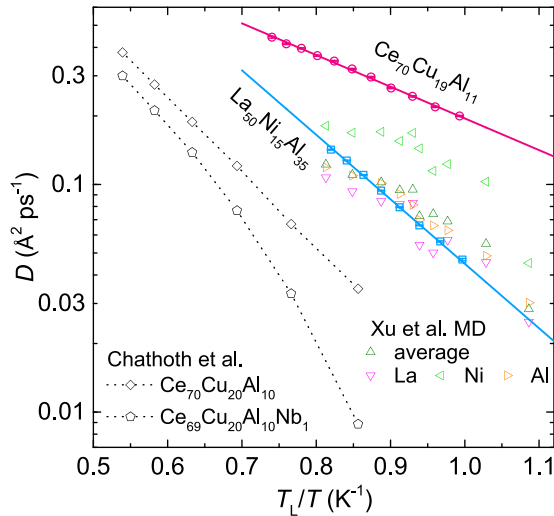


FIG. 5. Effective diffusion coefficient D as a function of the inversed temperature T_L/T for $\text{La}_{50}\text{Ni}_{15}\text{Al}_{35}$ (squares) and $\text{Ce}_{70}\text{Cu}_{19}\text{Al}_{11}$ (circles) melts, derived from the linear fits in Fig. 4. The error bars are within the size of the symbol. The straight lines are Arrhenius fits. The triangles are the molecular dynamics (MD) simulation data for $\text{La}_{50}\text{Ni}_{15}\text{Al}_{35}$ melt by Xu *et al.* [49]. The diamonds and pentagons are for $\text{Ce}_{70}\text{Cu}_{20}\text{Al}_{10}$ and $\text{Ce}_{69}\text{Cu}_{20}\text{Al}_{10}\text{Nb}_1$ melts, respectively, determined by quasielastic neutron scattering (QENS) by Chautho *et al.* [15]; the discrepancy from that in this paper was discussed in the context.

In Fig. 5 are also displayed the diffusion coefficients of the elements and their average in $\text{La}_{50}\text{Ni}_{15}\text{Al}_{35}$ from molecular dynamics (MD) simulation by Xu *et al.* [49] for comparison. In $\text{La}_{50}\text{Ni}_{15}\text{Al}_{35}$, the incoherent neutron scattering cross-section of Al is negligible; for Ni, it is 5.2 barn (1 barn = 10^{-28} m²); and for La, it is 1.13 barn. Considering the much larger atomic concentration of La, the scattered signals from the sample should be dominated by the incoherent contributions from both Ni and La atoms. Therefore, the measured diffusion coefficient is an average of these two elements, and we see that our measured data basically agree with the average diffusion coefficient evaluated from MD simulation in Ref. [49]. It has been suggested that, in $\text{La}_{50}\text{Ni}_{15}\text{Al}_{35}$, there could exist a change in activation energy of the diffusion coefficient accompanying a liquid-liquid phase transition around 1033 K [49]; however, this is not observed in our experimental data, which follow perfectly a single Arrhenius behavior in the entire temperature range of 973–1183 K.

Among the three elements in $\text{Ce}_{70}\text{Cu}_{19}\text{Al}_{11}$, only Cu has a marginal incoherent cross-section of 0.55 barn, and the other two are almost purely coherent scatterers. Therefore, the nominal coherent scattering from all elements could be comparable with the incoherent scattering from Cu in the studied Q range. Nevertheless, the elemental fluctuations are known to slow down the collective relaxation to the same level of the self-relaxation [17]. Therefore, the measured spectra are a combination of both incoherent and coherent scattering, and the obtained diffusion coefficient should be considered as an average of all constituent atoms in the system. Chautho *et al.* [15] reported QENS measurements for similar compositions of $\text{Ce}_{70}\text{Cu}_{20}\text{Al}_{10}$ and $\text{Ce}_{69}\text{Cu}_{20}\text{Al}_{10}\text{Nb}_1$ at higher

temperatures than ours, at 850–1350 K, but in contrast, they revealed diffusion coefficients over one order of magnitude smaller than ours. It has been demonstrated that, for Ce-based MGs, the glass-forming ability (GFA) is rather sensitive to microalloying [54,75] as well as the purity of the raw Ce material [76]. For instance, adding only 1–2% of Nb or Co in the $\text{Ce}_{70}\text{Cu}_{20}\text{Al}_{10}$ MG can result in an increase of the critical casting diameter from ~ 2 to ~ 10 mm, while changing the characteristic temperatures such T_g , T_L , and the crystallization temperature T_x by only a few degrees Kelvin [54,75]. Accordingly, Chautho *et al.* [15] observed a much smaller diffusion coefficient with non-Arrhenius temperature dependence in $\text{Ce}_{69}\text{Cu}_{20}\text{Al}_{10}\text{Nb}_1$ in contrast to $\text{Ce}_{70}\text{Cu}_{20}\text{Al}_{10}$ at the temperatures well above T_L (the data are represented in Fig. 5). More interestingly, Zhou *et al.* [76] recently found that a decrease in the purity of the raw Ce material by only 0.11% could result in as large as one order of magnitude increase of the GFA, thus expected to slow down the atomic dynamics of the alloy liquid. This is indeed consistent with the remarkable effect of microalloying on the GFA of Ce-based MGs and the stability of the corresponding supercooled liquids [50,54,75]. The composition of $\text{Ce}_{70}\text{Cu}_{19}\text{Al}_{11}$ in our study was verified by chemical analysis (Thermo IRIS Intrepid II XSP). It is unlikely that the difference between our results for $\text{Ce}_{70}\text{Cu}_{19}\text{Al}_{11}$ and that of Chautho *et al.* [15] for $\text{Ce}_{70}\text{Cu}_{20}\text{Al}_{10}$ comes from the 1% difference of Cu and Al because, even larger change of the composition of these elements has no significant effect on the GFA [54]. Therefore, it is possible that the purities of the raw Ce material used by Chautho *et al.* [15] and us are different, leading to the observed different results for the very similar nominal composition.

IV. CONCLUSIONS

In summary, our experimental observations show that liquid $\text{La}_{50}\text{Ni}_{15}\text{Al}_{35}$ and $\text{Ce}_{70}\text{Cu}_{19}\text{Al}_{11}$ in the equilibrium state exhibit stretched exponential relaxation and Arrhenius-type temperature dependence of the diffusion coefficient, in the temperature range of >200 K above their liquidus temperatures. The mean La/Ni self-diffusion in liquid $\text{La}_{50}\text{Ni}_{15}\text{Al}_{35}$ is slower and has much larger activation energy than the Cu self-diffusion in liquid $\text{Ce}_{70}\text{Cu}_{19}\text{Al}_{11}$, and it does not show any change of activation energy in the entire temperature range studied, in contrast to the previous observation associated with liquid-liquid phase transition [49]. Compared with $\text{La}_{50}\text{Ni}_{15}\text{Al}_{35}$ and most other metallic liquids, the $\text{Ce}_{70}\text{Cu}_{19}\text{Al}_{11}$ melt exhibits much more stretched relaxation behavior, suggestive of highly heterogeneous dynamics.

ACKNOWLEDGMENTS

This paper is supported by the U.S. Department of Energy (DOE), Office of Science, Office of Basic Energy Sciences, Materials Sciences and Engineering Division, under Award No. DE-SC0014084. This paper used resources at the Spallation Neutron Source, a DOE Office of Science User Facility operated by the Oak Ridge National Laboratory.

P.L. and A.J. contributed equally to this paper.

The authors declare no competing financial interest.

- [1] W. H. Wang, C. Dong, and C. H. Shek, *Mater. Sci. Eng. R Rep.* **44**, 45 (2004).
- [2] A. Inoue, *Acta Mater.* **48**, 279 (2000).
- [3] W. L. Johnson, *MRS Bull.* **24**, 42 (1999).
- [4] W. Klement, R. H. Willens, and P. Duwez, *Nature* **187**, 869 (1960).
- [5] M. Rappaz and W. J. Boettinger, *Acta Mater.* **47**, 3205 (1999).
- [6] W. J. Boettinger, J. A. Warren, C. Beckermann, and A. Karma, *Annu. Rev. Mater. Res.* **32**, 163 (2002).
- [7] K. F. Kelton, *Intermetallics* **14**, 966 (2006).
- [8] K. Binder and W. Kob, *Glassy Materials and Disordered Solids* (World Scientific, Singapore, 2011).
- [9] N. A. Mauro, M. Blodgett, M. L. Johnson, A. J. Vogt, and K. F. Kelton, *Nat. Commun.* **5**, 4616 (2014).
- [10] T. Egami, *Mod. Phys. Lett. B* **28**, 1430006 (2014).
- [11] T. Iwashita, D. M. Nicholson, and T. Egami, *Phys. Rev. Lett.* **110**, 205504 (2013).
- [12] J. S. Gardner, G. Ehlers, A. Faraone, and V. García Sakai, *Nat. Rev. Phys.* **2**, 103 (2020).
- [13] A. Jaiswal, A. Podlesnyak, G. Ehlers, R. Mills, S. O’Keeffe, J. Stevick, J. Kempton, G. Jelbert, W. Dmowski, K. Lokshin, T. Egami, and Y. Zhang, *Phys. Rev. B* **92**, 024202 (2015).
- [14] S. M. Chathoth and A. Podlesnyak, *J. Appl. Phys.* **103**, 013509 (2008).
- [15] S. M. Chathoth, B. Damaschke, J. P. Embs, and K. Samwer, *Appl. Phys. Lett.* **95**, 191907 (2009).
- [16] S. M. Chathoth, M. M. Koza, and A. Meyer, *Mater. Chem. Phys.* **136**, 296 (2012).
- [17] A. Jaiswal, S. O’Keeffe, R. Mills, A. Podlesnyak, G. Ehlers, W. Dmowski, K. Lokshin, J. Stevick, T. Egami, and Y. Zhang, *J. Phys. Chem. B* **120**, 1142 (2016).
- [18] C. Chen, K. Wong, R. P. Krishnan, L. Zhifeng, D. Yu, Z. Lu, and S. M. Chathoth, *J. Mater. Sci. Technol.* **35**, 44 (2019).
- [19] F. Yang, T. Unruh, and A. Meyer, *EPL* **107**, 26001 (2014).
- [20] A. Meyer, J. Wuttke, W. Petry, O. G. Randl, and H. Schober, *Phys. Rev. Lett.* **80**, 4454 (1998).
- [21] A. Meyer, R. Busch, and H. Schober, *Phys. Rev. Lett.* **83**, 5027 (1999).
- [22] S. M. Chathoth, A. Meyer, M. M. Koza, and F. Juranyi, *Appl. Phys. Lett.* **85**, 4881 (2004).
- [23] S. M. Chathoth, B. Damaschke, M. M. Koza, and K. Samwer, *Phys. Rev. Lett.* **101**, 037801 (2008).
- [24] P. Luo, Y. Zhai, E. Senses, E. Mamontov, G. Xu, Y. Z., and A. Faraone, *J. Phys. Chem. Lett.* **11**, 8970 (2020).
- [25] A. Jaiswal, T. Egami, K. F. Kelton, K. S. Schweizer, and Y. Zhang, *Phys. Rev. Lett.* **117**, 205701 (2016).
- [26] T. J. Lei, L. Rangel DaCosta, M. Liu, W. H. Wang, Y. H. Sun, A. L. Greer, and M. Atzmon, *Phys. Rev. E* **100**, 033001 (2019).
- [27] S. V. Ketov, Y. H. Sun, S. Nachum, Z. Lu, A. Checchi, A. R. Beraldin, H. Y. Bai, W. H. Wang, D. V. Louzguine-Luzgin, M. A. Carpenter, and A. L. Greer, *Nature* **524**, 200 (2015).
- [28] C. M. Meylan, J. Orava, and A. L. Greer, *J. Non. Cryst. Solids X* **8**, 100051 (2020).
- [29] Z. Lu, W. Jiao, W. H. Wang, and H. Y. Bai, *Phys. Rev. Lett.* **113**, 045501 (2014).
- [30] P. Luo, Z. Lu, Y. Z. Li, H. Y. Bai, P. Wen, and W. H. Wang, *Phys. Rev. B* **93**, 104204 (2016).
- [31] P. Luo, P. Wen, H. Y. Bai, B. Ruta, and W. H. Wang, *Phys. Rev. Lett.* **118**, 225901 (2017).
- [32] P. Luo, M. X. Li, H. Y. Jiang, P. Wen, H. Y. Bai, and W. H. Wang, *J. Appl. Phys.* **121**, 135104 (2017).
- [33] X. D. Wang, B. Ruta, L. H. Xiong, D. W. Zhang, Y. Chushkin, H. W. Sheng, H. B. Lou, Q. P. Cao, and J. Z. Jiang, *Acta Mater.* **99**, 290 (2015).
- [34] H. Y. Jiang, P. Luo, P. Wen, H. Y. Bai, W. H. Wang, and M. X. Pan, *J. Appl. Phys.* **120**, 145106 (2016).
- [35] P. Luo, Z. Lu, Z. G. Zhu, Y. Z. Li, H. Y. Bai, and W. H. Wang, *Appl. Phys. Lett.* **106**, 031907 (2015).
- [36] R. Zhao, H. Y. Jiang, P. Luo, L. Q. Shen, P. Wen, Y. H. Sun, H. Y. Bai, and W. H. Wang, *Phys. Rev. B* **101**, 094203 (2020).
- [37] H. Bin Yu, W. H. Wang, H. Y. Bai, and K. Samwer, *Natl. Sci. Rev.* **1**, 429 (2014).
- [38] J. C. Qiao, Y. H. Chen, R. Casalini, J. M. Pelletier, and Y. Yao, *J. Mater. Sci. Technol.* **35**, 982 (2019).
- [39] Z. G. Zhu, Z. Wang, and W. H. Wang, *J. Appl. Phys.* **118**, 154902 (2015).
- [40] L. Z. Zhao, R. J. Xue, Z. G. Zhu, K. L. Ngai, W. H. Wang, and H. Y. Bai, *J. Chem. Phys.* **144**, 204507 (2016).
- [41] Q. Wang, S. T. Zhang, Y. Yang, Y. D. Dong, C. T. Liu, and J. Lu, *Nat. Commun.* **6**, 7876 (2015).
- [42] L. Hu and Y. Yue, *J. Phys. Chem. C* **113**, 15001 (2009).
- [43] Y. Y. Bai, Y. L. Geng, C. M. Jiang, and B. Zhang, *J. Non. Cryst. Solids* **390**, 1 (2014).
- [44] Z. Wang, H. B. Yu, P. Wen, H. Y. Bai, and W. H. Wang, *J. Phys. Condens. Matter* **23**, 142202 (2011).
- [45] Z. G. Zhu, Y. Z. Li, Z. Wang, X. Q. Gao, P. Wen, H. Y. Bai, K. L. Ngai, and W. H. Wang, *J. Chem. Phys.* **141**, 084506 (2014).
- [46] Z. Wang, B. A. Sun, H. Y. Bai, and W. H. Wang, *Nat. Commun.* **5**, 5823 (2014).
- [47] B. Huang, Z. G. Zhu, T. P. Ge, H. Y. Bai, B. A. Sun, Y. Yang, C. T. Liu, and W. H. Wang, *Acta Mater.* **110**, 73 (2016).
- [48] H. B. Yu, X. Shen, Z. Wang, L. Gu, W. H. Wang, and H. Y. Bai, *Phys. Rev. Lett.* **108**, 015504 (2012).
- [49] W. Xu, M. T. Sandor, Y. Yu, H.-B. Ke, H.-P. Zhang, M.-Z. Li, W.-H. Wang, L. Liu, and Y. Wu, *Nat. Commun.* **6**, 7696 (2015).
- [50] B. Zhang, D. Q. Zhao, M. X. Pan, W. H. Wang, and A. L. Greer, *Phys. Rev. Lett.* **94**, 205502 (2005).
- [51] O. N. Senkov, *Phys. Rev. B* **76**, 104202 (2007).
- [52] Z. Lu, W.-H. Wang, and H.-Y. Bai, *Sci. China Mater.* **58**, 98 (2015).
- [53] B. Zhang, R. J. Wang, D. Q. Zhao, M. X. Pan, and W. H. Wang, *Phys. Rev. B* **70**, 224208 (2004).
- [54] B. Zhang, D. Q. Zhao, M. X. Pan, R. J. Wang, and W. H. Wang, *Acta Mater.* **54**, 3025 (2006).
- [55] G. Ehlers, A. A. Podlesnyak, and A. I. Kolesnikov, *Rev. Sci. Instrum.* **87**, 093902 (2016).
- [56] Throughout the paper, error bars of the raw data represent one standard deviation, and error bars of the fitted parameters represent one standard error, with 95% confidence interval.
- [57] See Supplemental Material at <http://link.aps.org/supplemental/10.1103/PhysRevB.103.224104> for Figs. S1–S6.
- [58] T. Scopigno, G. Ruocco, and F. Sette, *Rev. Mod. Phys.* **77**, 881 (2005).
- [59] H. P. Zhang, F. R. Wang, and M. Z. Li, *J. Phys. Chem. B* **123**, 1149 (2019).
- [60] A. Jaiswal, T. Egami, and Y. Zhang, *Phys. Rev. B* **91**, 134204 (2015).
- [61] A. Meyer, S. Stüber, D. Holland-Moritz, O. Heinen, and T. Unruh, *Phys. Rev. B* **77**, 092201 (2008).

- [62] A. Meyer, *Phys. Rev. B* **81**, 012102 (2010).
- [63] F. Kargl, H. Weis, T. Unruh, and A. Meyer, *J. Phys. Conf. Ser.* **340**, 012077 (2012).
- [64] A. Meyer, *EPJ Web Conf.* **83**, 01002 (2015).
- [65] F. Demmel, D. Szubrin, W.-C. Pilgrim, and C. Morkel, *Phys. Rev. B* **84**, 014307 (2011).
- [66] A. Meyer, J. Horbach, O. Heinen, D. Holland-Moritz, and T. Unruh, *Defect Diffus. Forum* **289–292**, 609 (2009).
- [67] S. Szabó and Z. Evenson, *Appl. Phys. Lett.* **110**, 161903 (2017).
- [68] F. Yang, D. Holland-Moritz, J. Gegner, P. Heintzmann, F. Kargl, C. C. Yuan, G. G. Simeoni, and A. Meyer, *EPL* **107**, 46001 (2014).
- [69] U. Dahlborg, M. Besser, M. Calvo-Dahlborg, S. Janssen, F. Juranyi, M. J. Kramer, J. R. Morris, and D. J. Sordelet, *J. Non. Cryst. Solids* **353**, 3295 (2007).
- [70] J. Horbach, S. K. Das, A. Griesche, M. P. Macht, G. Froberg, and A. Meyer, *Phys. Rev. B* **75**, 174304 (2007).
- [71] D. Holland-Moritz, S. Stüber, H. Hartmann, T. Unruh, T. Hansen, and A. Meyer, *Phys. Rev. B* **79**, 064204 (2009).
- [72] B. Nowak, D. Holland-Moritz, F. Yang, T. Voigtmann, Z. Evenson, T. C. Hansen, and A. Meyer, *Phys. Rev. B* **96**, 054201 (2017).
- [73] J. Brillo, S. M. Chathoth, M. M. Koza, and A. Meyer, *Appl. Phys. Lett.* **93**, 121905 (2008).
- [74] A. Arbe, J. Colmenero, M. Monkenbusch, and D. Richter, *Phys. Rev. Lett.* **81**, 590 (1998).
- [75] B. Zhang, R. J. Wang, D. Q. Zhao, M. X. Pan, and W. H. Wang, *Phys. Rev. B* **73**, 092201 (2006).
- [76] Y. Zhou, Y. Zhao, B. Y. Qu, L. Wang, R. L. Zhou, Y. C. Wu, and B. Zhang, *Intermetallics* **56**, 56 (2015).